ACS APPLIED MATERIALS & INTERFACES

Research Article

www.acsami.org

Crystalline GaSb Nanowires Synthesized on Amorphous Substrates: From the Formation Mechanism to p-Channel Transistor Applications

Zai-xing Yang,[†,‡] Fengyun Wang,[†,§,‡] Ning Han,[†,#,‡] Hao Lin,[†] Ho-Yuen Cheung,[⊥] Ming Fang,[†] SenPo Yip,[†,#] TakFu Hung,[†] Chun-Yuen Wong,[⊥] and Johnny C. Ho*[,†,#]

[†]Department of Physics and Materials Science and [⊥]Department of Biology and Chemistry, City University of Hong Kong, 83 Tat Chee Avenue, Kowloon, Hong Kong

[§]Cultivation Base for State Key Laboratory, Qingdao University, No. 308 Ningxia Road, Qingdao, People's Republic of China

[#]Shenzhen Research Institute, City University of Hong Kong, Shenzhen, People's Republic of China

Supporting Information

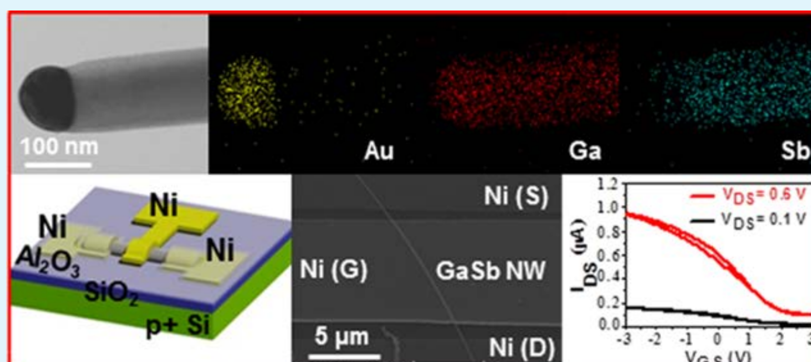

ABSTRACT: In recent years, because of the narrow direct bandgap and outstanding carrier mobility, GaSb nanowires (NWs) have been extensively explored for various electronics and optoelectronics. Importantly, these p-channel nanowires can be potentially integrated with n-type InSb, InAs, or InGaAs NW devices via different NW transfer techniques to facilitate the III−V CMOS technology. However, until now, there have been very few works focusing on the electronic transport properties of GaSb NWs. Here, we successfully demonstrate the synthesis of crystalline, stoichiometric, and dense GaSb NWs on amorphous substrates, instead of the commonly used III−V crystalline substrates, InAs, or GaAs NW stems as others reported. The obtained NWs are found to grow via the VLS mechanism with a narrow distribution of diameter (220 ± 50 nm) uniformly along the entire NW length (>10 μm) with minimal tapering and surface coating. Notably, when configured into FETs, the NWs exhibit respectable electrical characteristics with the peak hole mobility of ~30 $cm^2 V^{-1} s^{-1}$ and free hole concentration of ~9.7 × 10^{17} cm^{-3}. All these have illustrated the promising potency of such NWs directly grown on amorphous substrates for various technological applications, as compared with the conventional MOCVD-grown GaSb NWs.

KEYWORDS: *GaSb, nanowires, p-channel, field-effect transistors, hole mobility, hole concentration*

1. INTRODUCTION

In the past decades, because of unique physical and chemical properties, one-dimensional (1D) semiconductor nanowires (NWs) have attracted extensive research attention as fundamental building blocks for next-generation electronic, optoelectronic, and photovoltaic devices.[1−8] In particular, III−Sb NW materials are intriguing for their large Bohr exciton radius, narrow direct bandgaps and excellent carrier mobilities, with InSb and GaSb having the highest electron and hole mobility, respectively, among all III−Vs, making them ideal materials for field-effect transistors (FETs), quantum devices, thermoelectrics and long-wavelength detectors, etc.[9−15] For example, single hole transistors (SHTs) have been recently demonstrated and made from p-type GaSb NWs in which the long coherence time for spin hole states enable these SHTs promising for spintronic applications.[10,16] At the same time, these high-performance p-type GaSb NWs can also be potentially integrated with n-type InSb, InAs or InGaAs NW devices via different NW transfer techniques to facilitate the III−V complementary metal-oxide-semiconductor (CMOS) technology.[14] In any case, although these p-type NW material is essential to the establishment of various breakthroughs, there have been very few reports on the development of p-type GaSb NWFETs until now, possibly because of the challenges in the

Received: July 31, 2013
Accepted: October 9, 2013
Published: October 9, 2013

 © 2013 American Chemical Society

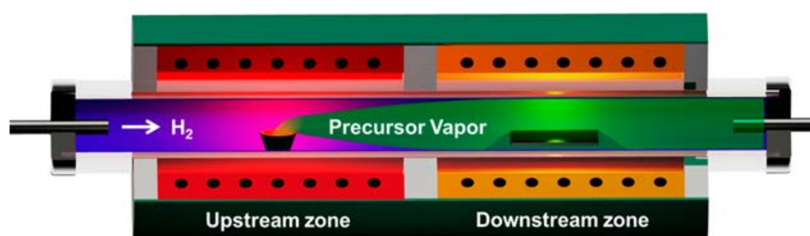

Figure 1. Schematic representation of the CVD setup and the growth process.

growth of high crystal quality and controllable surface condition of these NWs.[17,18] Typically, because of the surfactant effect, the constituent Sb tends to aggregate on top of the growing layer without being incorporated into the NW growth, resulting in a strong influence on the interfacial energies for the NW nucleation from catalyst particles.[19,20] This way, a much higher concentration of the precursor vapors (group III[21,22] and possible group V atoms[23,24]) is always required for this NW growth and easily yielded uncontrollable radial growth even for a small local variation in the V/III ratio.[25] In this report, we demonstrate a successful synthesis technique utilizing Au nanoclusters (NCs) as the catalysts to achieve high density GaSb NWs on amorphous Si/SiO_2 substrates via solid-source chemical vapor deposition (SSCVD). The obtained NWs are stoichiometric, single-crystalline with a smooth surface, very uniform in diameter, and following the vapor-liquid-solid (VLS) growth mode. More importantly, these grown NWs exhibit good p-channel device performance when configured as FETs, with one of the respectable peak hole mobilities (~30 $cm^2\ V^{-1}\ s^{-1}$) reported so far for GaSb NWs.[26−30]

2. EXPERIMENTAL SECTION

Nanowire Synthesis. GaSb NWs studied in this work were grown by employing SSCVD scheme with the solid GaSb (99.999% purity) powder as the source materials. Briefly, a dual-zone horizontal tube furnace, one zone for the solid source (upstream) and one zone for the growth substrate (downstream), was used as the reactor for the synthesis of GaSb NWs. At first, Si/SiO_2 substrate pieces (50 nm thick thermal grown oxide; size of 1 cm × 5 cm) pre-deposited with a thin layer of Au (1 nm nominal thickness) was placed in the middle of the downstream zone and thermally annealed at 800 °C for 10 mins in a hydrogen environment (0.18 Torr) to obtain Au nanocrystals (NCs) as the catalyst. The solid source, GaSb powders placed within a boron nitride crucible, was positioned in the upstream zone with a distance of 15 cm away from the sample. During the growth, the source and substrate were heated to the temperatures of 800−900 °C and 500−640 °C respectively for growth optimization. Hydrogen (99.9995% purity; 30 sccm) was used as the carrier gas to transport the thermally vaporized precursors to the downstream, and the pressure was maintained at 0.18 Torr for the entire duration of the growth (0.5 h). Prior to heating, the quartz tube was purged with H_2 for 0.5 h. After the growth, the source and substrate heater were stopped together and cooled to room temperature under the hydrogen flow without rapid cooling by opening the cover of the furnace. In this case, the NWs were grown chemically intrinsic without any intentional dopants with the growth setup illustrated in Figure 1.

Characterization Methods. Surface morphologies of the grown NWs were examined with a scanning electron microscope (SEM, FEI/Philips XL30 Esem-FEG) and a transmission electron microscope (TEM, Philips CM-20). Crystal structures were determined by collecting XRD patterns on a Philips powder diffractometer using Cu Kα radiation (λ = 1.5406 Å), imaging with a high resolution TEM (HRTEM, JEOL 2100F, JEOL Co., Ltd., Tokyo, Japan) and selected area electron diffraction (SAED, Philips CM-20). Elemental mappings were performed using an energy dispersive X-ray spectroscopy (EDS) detector attached to the JEOL 2100F to measure the chemical composition of the grown NWs. For the TEM and elemental mappings, the NWs were first suspended in ethanol (absolute) by ultrasonication and drop-casted onto the grid for the corresponding characterization. For the cross-sectional HRTEM observation, the NWs were dispersed in a resin, which was then cut into ~25 nm slices after being dried and supported by a copper grid.

Nanowire FET Fabrication and Measurements. The NW electrical device performance was studied based on both back-gated and top-gated FET configuration. The obtained NW suspension was drop-casted onto highly doped p-type Si substrates with a 50 nm thick thermally grown gate oxide. Photolithography was then utilized to define the source and drain regions, and 80-nm thick Ni film was thermally deposited as the contact electrodes followed by a lift-off process for the fabrication of back-gated devices. While for top-gated FETs, an addition dielectric layer of 25 nm thick Al_2O_3 was thermally evaporated on top of the attained structure, with a 10 h annealing at 100 °C in ambient to densify the top dielectrics. A second photolithography was performed to define the top-gate regions and 80 nm thick Ni film was thermally deposited as the contact electrodes followed by a lift-off process. Electrical performance of the fabricated devices was characterized with a standard electrical probe station and Agilent 4155C semiconductor analyzer (Agilent Technologies, CA, USA).

3. RESULTS AND DISCUSSION

Morphology and Crystal Structure. As shown in the SEM image (Figure 2a), after a detailed investigation in the growth parameters such as the source/substrate temperatures, very dense, long (>10 μm) and straight GaSb NWs is successfully obtained with the optimized growth process (source temperature = 850 °C and substrate temperature = 620 °C) for NW length, density, and surface morphology on the amorphous Si/SiO_2 substrate, instead of the commonly utilized crystalline III−V crystals,[12] InAs,[9,31,32] or GaAs NW stems.[21,33] On the basis of the XRD spectrum (Figure 2b), the detected peaks are identical to those of the cubic zincblende (ZB) structure of GaSb, having $a = b = c$ = 0.6095 nm (JCPDS Card No. 07-0215) with no peaks associated with the hexagonal wurtzite (WZ) structure. The phase purity is also high as there is no indication of other phases such as those of Ga_2O_3, excess elemental Ga and Sb. Moreover, optical absorption measurement is performed to assess the band gap energy of the grown NWs for wavelengths from 1200 to 1850 nm (Figure 2c). The absorption edge is determined at around 1679 nm (~0.74 eV) and is comparable to the one of bulk ZB GaSb material (0.72 eV); therefore, these obtained NWs can enable optoelectronic applications in the infrared (IR) regions.

It is also noted that significant surface coating and tapering induced from the excessive radial growth would be observed for the NWs grown with any deviation from this optimized condition (Supporting Information, Figure S1), which can be attributed to the imbalance of the V/III precursor ratio supplied during the growth as well as the inappropriate growth

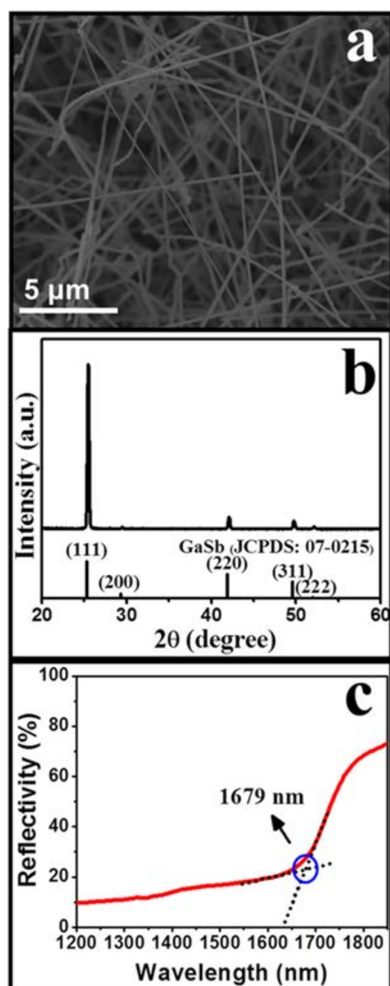

Figure 2. (a) SEM image of the as-prepared GaSb NWs grown with the optimal process condition, (b) corresponding XRD spectrum, and (c) reflectance spectrum of GaSb NWs for wavelengths from 1200 to 1850 nm. (Optimal growth conditions: source temperature at 850 °C, growth temperature at 620 °C, pressure at 0.18 Torr, gas flow rate at 20 sccm, and growth duration for 0.5 h).

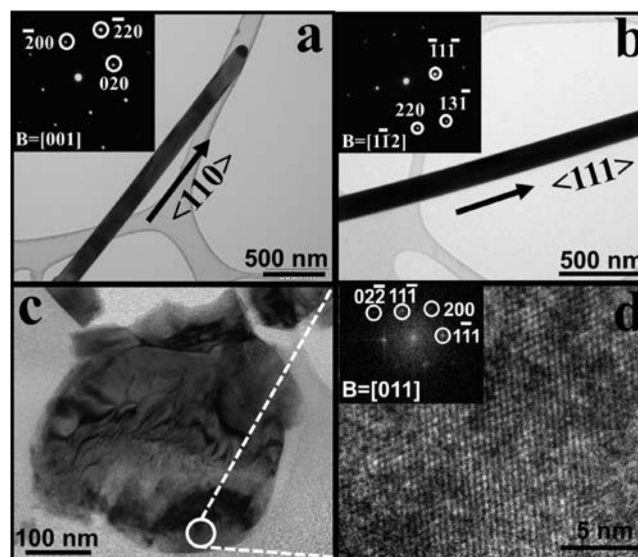

Figure 3. (a, b) Typical TEM images of individual GaSb NWs and the corresponding SAED images illustrating the growth direction of ⟨110⟩ and ⟨111⟩, respectively; (c, d) radial cross-sectional TEM and HRTEM images of a representative NW (NW diameter ~300 nm).

temperature.[14,19,34] Although the V/III ratio cannot be directly and independently manipulated in this simple SSCVD technique, it can rather be tailored by adjusting the source temperature, growth time and carrier gas flow rate altogether. Because there is a substantial vapor pressure difference between the constituents Ga and Sb, this large difference is believed to induce a supersaturated Sb environment required[14] for the growth of high-quality GaSb NWs before the Sb source gets depleted. In this regard, our NWs are grown with short growth time (0.5 h) to aim for reduced uncontrollable radial growth without sacrificing much on the NW length and density. Any growth performed longer than 0.5 h would lead to surface coating and tapering of NWs. With this optimized condition, Figure 3a depicts a typical TEM image of an individual GaSb NW growing along ⟨110⟩ direction with the spherical catalytic tip, which clearly demonstrates that the diameter is uniform along the NW without any tapering observed. The single-crystallinity is also confirmed by the corresponding SAED pattern. In general, the obtained NWs have an average diameter of 220 ± 50 nm from the statistics of more than 100 NWs studied from the TEM images and this is comparable to the variation of commercially available colloidal Au NCs for growing NWs (~10 to 15 %). In this work, small diameter NWs have been explored as well with the use of thinner Au catalyst film (i.e., 0.2 nm nominal thickness); however, significant surface coating or uncontrollable radial growth is observed (see the Supporting Information, Figure S2), agreeing well with the Gibbs−Thomson model[14,35,36] that Sb supersaturation in the catalytic NCs is reduced due to the high Sb vapor pressure in small diameter NCs. This way, higher precursor partial pressures are needed for the NW nucleation and easily yield the uncontrolled overgrowth.[14] Although GaSb NWs with the diameter down to 32 nm have been epitaxially grown on InAs stems ($d \approx 21$ nm),[18] their NW catalytic supersaturation processes are dissimilar from our non-epitaxial case, especially there is not any lattice registration effect in minimizing anisotropic crystal free energies during our NW nucleation stage.[37] This way, the achievable critical NW diameters would be different between the epitaxial and non-epitaxial growth.

To further evaluate the NW crystal quality, we performed cross-sectional HRTEM of a representative NW (Figure 3c). It is worth pointing out that the distorted pattern in this cross-sectional image is brought up by the sample preparation process, where the NWs are cut into very thin slices (~25 nm in the thickness) and the lattice might be destroyed. Based on the plane spacing determination (Figure 3d) and corresponding reciprocal lattice space extracted by fast fourier transform (FFT), the NW exhibit good crystallinity, growth orientation in ⟨110⟩ direction, and with no significant crystal defects. Typically, the growth orientation of ⟨111⟩ direction is commonly observed for III−V NWs because of the lowest surface energy of {111} planes favoring the crystal growth for the NW formation.[38] In any case, both ⟨110⟩- and ⟨111⟩-oriented NWs are observed here (Figure 3b) roughly with the equal fraction in which the ⟨110⟩ NW is probably induced by the defect formation in the initial stage of the NW growth, favoring the next higher index directions.[14]

Stoichiometry and Growth Mechanism. Moreover, one of the challenges in synthesizing high-quality III−V NWs is to

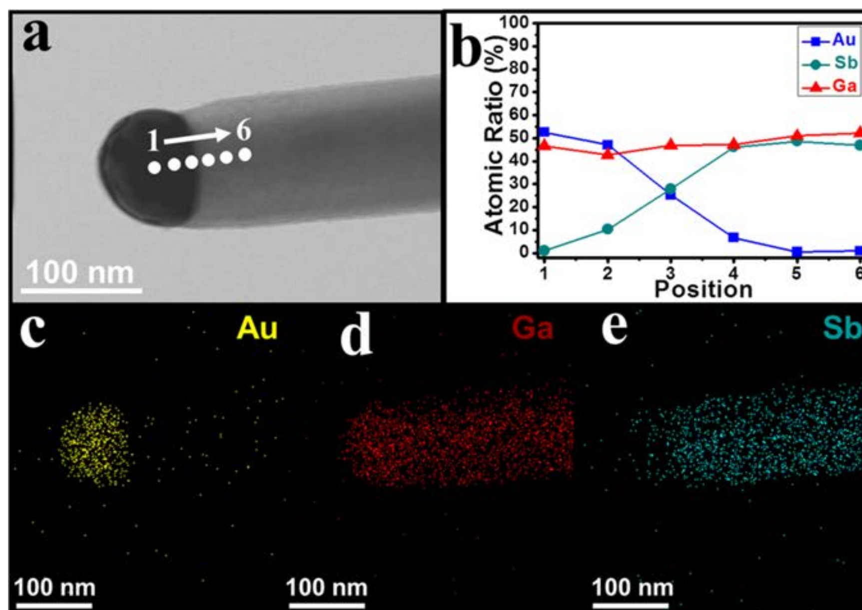

Figure 4. (a) Scanning TEM image of an individual GaSb NWs; (b) EDS line scan (measured from the position 1 to 6, as indicated by the white arrow in panel a of a representative as-grown GaSb NW tip region; (c−e) EDS elemental mappings of the corresponding NW for Au, Ga, and Sb atoms.

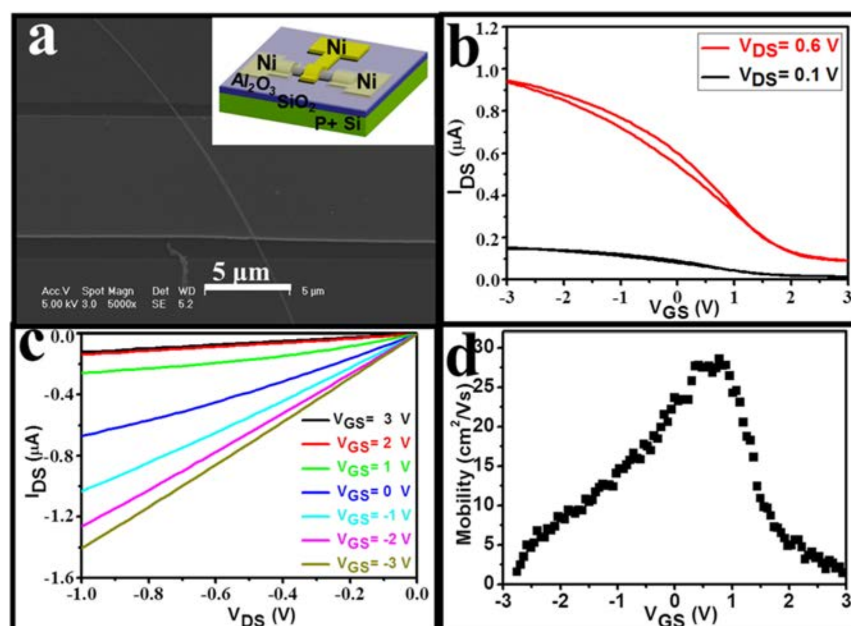

Figure 5. (a) SEM image and (inset) schematic of a top-gated GaSb NWFET with Ni metal contacts and gate; (b, c) transfer and output characteristics of the representative NWFET; (d) mobility assessment under V_{DS} = 0.1 V of the device presented in the panel a. The back-gate bias is set at −10 V for all measurements here.

control the NW stoichiometry uniformly to enable various device applications. As presented in Figure 4c−e, the EDS elemental mapping of the same NW (Figure 4a) illustrates the homogeneous distribution of Au, Ga, and Sb atoms along the NW body. In order to quantify the corresponding chemical composition, the line scan is also performed along the NW axial direction across from the tip to the body (Figure 4b). It is found that the catalyst tip mainly contains Ga and Au atoms (atomic ratio ≈ 1:1), whereas the Au content drops drastically once passing the catalyst/NW interface. However, because the detection limit of EDS is usually within 1−2%, which is far higher than the typical doping levels, the residual Au content may still exist in affecting the electrical properties of nanowires here. At the same time, one can also see that the NW body consists of Ga and Sb elements in the atomic ratio of 1:1, suggesting that the stoichiometric GaSb NWs are catalyzed by GaAu alloy tips. According to the binary phase diagram of Au and Ga, the melting point of bulk AuGa is about 461 °C[39] and under the nano-size effect as well as the low pressure condition,[40,41] the melting point of the AuGa alloy would be further reduced. This way, the AuGa alloy catalyst is believed to exist in liquid phase at our growth temperature of (620 °C),

Table 1. Comparison of Various Electrical Properties among p-Type III−V Nanowire Devices

materials	growth method	doped/un-doped	peak mobility ($cm^2/(V\ s)$)	resistivity (Ω cm)	concentration (cm^{-3})	diameter (nm)	ref
GaSb	MOVPE	undoped		0.2−0.4		100	26
GaSb	MOCVD	undoped		0.23 ± 0.18		91	29
GaSb	CVD	undoped	14.2		2.2×10^{18}	130	30
GaSb	**CVD**	**undoped**	**30**	**0.23 (ungated; V_{GS} = 0 V)** **0.15 (gated; V_{GS} = −3 V)**	**9.7×10^{17}**	**180**	**our work**
GaAs	MOVPE	Zn-doped	90		1.7×10^{19}	75	44
InAs	CVD	Zn-doped	60	0.02	1.0×10^{19}	30	2
InAs	MBE	Be-doped	1		3×10^{18}	73	45
InSb	CVD	C-doped	140		7.5×10^{17}	55	46

whereas the spherical shape of observed tips further provide evidence of the molten catalyst in the liquid state. Furthermore, the finding that no detectable Sb concentration is found in the tip indicates that the solubility of Sb in Au eutectoids is relatively low and Sb atoms would react in the tip/NW interface to induce the NW growth via VLS mechanism (see the Supporting Information, Figure S3). All these demonstrate the well-controlled surface morphology, crystallinity and stoichiometry of NWs achieved with this simple growth technique as compared with the sophisticated MOCVD systems.

Electrical Characteristics and Device Performances. To shed light and assess the electrical properties of our NWs, we first fabricated single NW as well as parallel NW array FETs with the global back-gated configuration. Because the grown NWs have relatively large diameters, the gate-coupling is not effective here such that the device capacitance as well as the output current (I_{DS}) cannot be modulated efficiently (see the Supporting Information, Figure S4); as a result, the top-gated device geometry is adopted. Figure 5a illustrates the top view SEM image and schematic of the representative FET with the NW diameter of $d \approx 180$ nm and a gate length of $L \approx 9$ μm (distance between source/drain ~11 μm). The corresponding transfer and output characteristics are shown in Figure 5b, c, respectively. It is obvious that the device exhibit p-channel conductivity with a minimal hysteresis and delivers ~950 nA ON current under V_{DS} = 0.6 V, V_{GS} = −3 V and ~160 nA ON current under V_{DS} = 0.1 V, V_{GS} = −3 V. Also, the linear I_{DS}−V_{DS} behavior further confirms that the Ni contacts to the p-GaSb are nearly ohmic. Meanwhile, the corresponding field-effect hole mobility can be calculated as a function of V_{GS} (Figure 5d). Specifically, the transconductance ($g_m = (dI_{DS})/(dV_{GS})|V_{DS}$) at low bias V_{DS} = 0.1 V is assessed and the mobility is deduced by the standard square law model $\mu = g_m(L^2/C_{OX})(1/V_{DS})$, where C_{OX} is the gate capacitance and L is the channel length.[40] It is worth mentioning that the C_{OX} is obtained from the finite element analysis software COMSOL tailored for this geometry with the details given in the Supporting Information, Figure S5. For the dielectric thickness of 25 nm, NW diameter of 180 nm and channel length of 9 μm, the effective gate capacitance is estimated as ~14.13 fF, the peak transconductance is approximated as $\sim 5 \times 10^{-8}$ S (see the Supporting Information, Figure S6) and the peak hole mobility is found to be ~30 $cm^2\ V^{-1}\ s^{-1}$. For a statistic of more than 10 NW devices with similar diameters, which would involve both ⟨111⟩ and ⟨110⟩ oriented NWs, the average mobility is compiled as 21.2 ± 5.9 $cm^2\ V^{-1}\ s^{-1}$. This variation can be attributed to the dependence of electrical properties on NW orientation, surface roughness, and others, while current investigations are ongoing.

Similarly, the effective hole concentration can also be assessed from the total charge in the NW, $n_h = Q/(q\pi r^2 L) = (C_{OX}V_{th})/(q\pi r^2 L)$, where r is the NW radius and V_{th} is the threshold voltage. This way, for the rough estimation of threshold voltage at 2.5 V and the same values of C_{OX} and L, the hole concentration can be approximated as $\sim 9.7 \times 10^{17}$ cm^{-3}, comparable to the lowest values reported in the literature,[14,30] indicating the reasonably good crystal quality of our NWs. This free carrier concentration is believed to originate from the prevalence of native crystal defects such as Ga_{Sb} antisite or Ga vacancy.[19] In any case, the current density and carrier concentration can be manipulated in the future by incorporating p-type dopants like zinc or carbon during the growth and employing better electrical contact schemes.[42,43] All these results demonstrate the profound potency of our solid-source CVD grown GaSb NWs for various electronic and optoelectronic applications.

Moreover, electrical properties of the obtained GaSb NWs are also contrasted with the ones of other p-type III−V NWs reported in the literature. As shown in Table 1, our NWs exhibit an ungated resistivity of 0.23 Ω cm (see the Supporting Information) which is similar to those of other GaSb NWs, indicating the successful synthesis of comparable GaSb NWs via this simple solid-source CVD technique developed in this work. When the NW FET is operated in the ON-state, the resistivity is decreased to 0.15 Ω cm (see the Supporting Information) while this reduction in the resistivity is predicted in this depletion mode device as the gate would induce the accumulation of carriers for efficient charge conduction in the NW channel. In any case, our NWs have displayed respectable peak mobilities among all GaSb NWs and comparable electrical performances with p-type GaAs, InAs and InSb NWs, etc. Notably, further enhancement can be achieved by utilizing other catalysts (e.g., Ni or Ga) in order to eliminate the formation of deep-level defect states by residual Au in deteriorating the NW electrical properties, improving the gate electrostatic control by scaling the NW diameter as well as enhancing the NW surface condition such as roughness and NW/dielectric interface properties through the adoption of high quality atomic layer deposited (ALD) dielectric layer.

4. CONCLUSIONS

In summary, we have illustrated a simple CVD technique utilizing Au NCs as the starting catalysts to synthesize highly-dense, long and straight GaSb NWs with smooth surface on amorphous Si/SiO_2 substrates via the VLS growth mechanism. The obtained NWs are crystalline and stoichiometric with

uniform diameters as well as minimal surface coatings. When configured into FETs, the NWs exhibit respectable p-channel device characteristics with the peak hole mobility of ~30 cm^2 V^{-1} s^{-1} and effective hole concentration of ~9.7×10^{17} cm^{-3}, in which the performance is believed to get further improved by the NW diameter scaling and the utilization of other catalysts as well as high quality ALD dielectrics. All these have indicated the significant potential implications of our GaSb NWs for various technological applications.

■ ASSOCIATED CONTENT

Supporting Information

Optimization of NW growth parameters; investigation of small diameter NWs; NW growth mechanism; global back-gated single NW and parallel NW array FETs; COMSOL simulation for the gate capacitance determination; transconductance and resistivity calculation. This material is available free of charge via the Internet at http://pubs.acs.org.

■ AUTHOR INFORMATION

Corresponding Author

*E-mail: johnnyho@cityu.edu.hk.

Author Contributions

‡Z.Y., F.W., and N.H. contributed equally to this work.

Notes

The authors declare no competing financial interest.

■ ACKNOWLEDGMENTS

This research was supported by the General Research Fund of the Research Grants Council of Hong Kong SAR, China, under project number CityU 101111, the National Natural Science Foundation of China (Grant 51202205), the Guangdong National Science Foundation (Grant S2012010010725), the Science Technology and Innovation Committee of Shenzhen Municipality (Grant JCYJ20120618140624228), and was supported by a grant from the Shenzhen Research Institute, City University of Hong Kong.

■ REFERENCES

(1) Gudiksen, M. S.; Lauhon, L. J.; Wang, J.; Smith, D. C.; Lieber, C. M. *Nature* **2002**, *415*, 617−620.
(2) Ford, A. C.; Chuang, S.; Ho, J. C.; Chueh, Y. L.; Javey, A. *Nano Lett.* **2010**, *10*, 509−513.
(3) Lupan, R. O.; Pauporté, T.; Viana, B.; Tiginyanu, I. M.; Ursaki, V. V.; Cortès, R. *ACS Appl. Mater. Interfaces* **2010**, *2*, 2083−2090.
(4) Alamo, J. A. *Nature* **2011**, *479*, 317−323.
(5) Weng, W. Y.; Chang, S. J.; Hsu, C. L.; Hsueh, T. J. *ACS Appl. Mater. Interfaces* **2011**, *3*, 162−166.
(6) Hou, J. J.; Han, N.; Wang, F.; Xiu, F.; Yip, S.; Hui, A. T.; Hung, T.; Ho, J. C. *ACS Nano* **2012**, *6*, 3624−3630.
(7) Wu, P. M.; Anttu, N.; Xu, H.; Samuelson, L.; Pistol, M. E. *Nano Lett.* **2012**, *12*, 1990−1995.
(8) Han, N.; Wang, F. Y.; Hou, J. J.; Yip, S. Y.; Lin, H.; Xiu, F.; Fang, M.; Yang, Z. X.; Shi, X. L.; Dong, G. F.; Hung, T. F.; Ho, J. C. *Adv. Mater.* **2013**, *25*, 4445−4451.
(9) Borg, B. M.; Dick, K. A.; Ganjipour, B.; Pistol, M. E.; Wernersson, L. E.; Thelander, C. *Nano Lett.* **2010**, *10*, 4080−4085.
(10) Ganjipour, B.; Nilsson, H. A.; Borg, B. M.; Wernersson, L. E.; Samuelson, L.; Xu, H. Q.; Thelander, C. *Appl. Phys. Lett.* **2011**, *99*, 262104.
(11) Dey, A. W.; Svensson, J.; Borg, B. M.; Ek, M.; Wernersson, L. E. *Nano Lett.* **2012**, *12*, 5593−5597.
(12) Yan, C. L.; Li, X. P.; Zhou, K. Y.; Pan, A. L.; Werner, P.; Mensah, S. L.; Vogel, A. T.; Schmidt, V. *Nano Lett.* **2012**, *12*, 1799−1805.
(13) Xu, W.; Chin, A.; Ye, L.; Ning, C. Z.; Yu, H. *J. Appl. Phys.* **2012**, *111*, 104515.
(14) Borg, B. M.; Wernersson, L. E. *Nanotechnology* **2013**, *24*, 202001.
(15) Bandyopadhyay, S.; Anderson, J. *Appl. Phys. Lett.* **2013**, *102*, 103108.
(16) Zhang, W.; Dobrovitski, V. V.; Al-Hassanieh, K. A.; Daggoto, E.; Harmon, B. N. *Phys. Rev. B* **2006**, *74*, 205313.
(17) Zi, Y. L.; Zhao, Y. J.; Candebat, D.; Appenzeller, J.; Yang, C. *ChemPhysChem* **2012**, *13*, 2585−2588.
(18) Ek, M.; Borg, B. M.; Johansson, J.; Dick, K. A. *ACS Nano* **2013**, *7*, 3668−3675.
(19) Aardvark, A.; Mason, N. J.; Walker, P. J. *Prog. Cryst. Growth Charact.* **1997**, *35*, 207−241.
(20) Dimroth, F.; Agert, C.; Bett, A. W. *J. Cryst. Growth* **2003**, *248*, 265−273.
(21) Jeppsson, M.; Dick, K. A.; Wagner, J. B.; Caroff, P.; Deppert, K.; Samuelson, L.; Wernersson, L. *J. Cryst. Growth* **2008**, *310*, 4115−4121.
(22) Caroff, P.; Messing, M. E.; Borg, B. M.; Dick, K. A.; Deppert, K.; Wernersson, L.E. *Nanotechnology* **2009**, *20*, 495606.
(23) Pozuelo, M.; Zhou, H.; Lin, S.; Lipman, S. A.; Goorsky, M. S.; Hicks, R. F.; Kodambaka, S. *J. Cryst. Growth* **2011**, *329*, 6−11.
(24) Mandl, B.; Dick, K. A.; Kriegner, D.; Keplinger, M.; Bauer, G.; Stangl, J.; Deppert, K. *Nanotechnology* **2011**, *22*, 145603.
(25) Plissard, S. R.; Slapak, D. R.; Verheijen, M. A.; Hocevar, M.; Immink, G. W. G.; van Weperen, I.; Nadj-Perge, S.; Frolov, S. M.; Kouwenhoven, L. P.; Bakkers, E. P. A. M. *Nano Lett.* **2012**, *12*, 1794−1798.
(26) Burke, R. A.; Weng, X. J.; Kuo, M. E.; Song, Y. W.; Itsuno, A. M.; Mayer, T. S.; Durbin, S. M.; Reeves, R. J.; Redwing, J. M. *J. Electron Mater.* **2010**, *39*, 355−364.
(27) Ganjipour, B.; Ek, M.; Borg, B. M.; Dick, K. A.; Pistol, M. E.; Wernersson, L. E.; Thelander, C. *Appl. Phys. Lett.* **2012**, *101*, 103501.
(28) Vaddiraju, S.; Sunkara, M. K.; Chin, A. H.; Ning, C. Z.; Dholakia, G. R.; Meyyappan, M. *J. Phys. Chem. C* **2007**, *111*, 7339−7347.
(29) Jeppsson, M.; Dick, K. A.; Nilsson, H. A.; Sköld, N.; JWagner, J. B.; Caroff, P.; Wernersson, L. E. *J. Cryst. Growth* **2008**, *310*, 5119−5122.
(30) Xu, G. W.; Huang, S. Y.; Wang, X. Y.; Yu, B.; Zhang, H.; Yang, T.; Xu, H. Q.; Dai, L. *RSC Adv.* **2013**, *3*, 19834−19839.
(31) Ek, M.; Borg, B. M.; Dey, A. W.; Ganjipour, B.; Thelander, C.; Wernersson, L. E.; Dick, K. A. *Cryst. Growth Des.* **2011**, *11*, 4588−4593.
(32) Dey, A. W.; Svensson, J.; Borg, B. M.; Ek, M.; Wernersson, L. E. *Nano Lett.* **2012**, *12*, 5593−5597.
(33) Guo, Y. N.; Zou, J.; Paladugu, M.; Wang, H.; Gao, Q.; Tan, H. H.; Jagadish, C. *Appl. Phys. Lett.* **2006**, *89*, 231917.
(34) Han, N.; Wang, F. Y.; Hui, A. T.; Hou, J. J.; Shan, G. C.; Fei, X.; Hung, T. F.; Ho, J. C. *Nanotechnology* **2011**, *22*, 285607.
(35) Johansson, J.; Svensson, C. P. T.; Mårtensson, T.; Samuelson, L.; Seifert, W. M. *J. Phys. Chem. B* **2005**, *109*, 13567−13571.
(36) Han, N.; Wang, F. Y.; Hou, J. J.; Yip, S. P.; Lin, H.; Fang, M.; Xiu, F.; Shi, X.; Hung, T. F.; Ho, J. C. *Cryst. Growth Des.* **2012**, *12*, 6243−6249.
(37) Chung, H. S.; Jung, Y.; Kim, S. C.; Kim, D. H.; Oh, K. H.; Agarwa, R. *Nano Lett.* **2009**, *9*, 2395−2401.
(38) Seifert, W.; Borgström, M.; Deppert, K.; Dick, K. A.; Johansson, J.; Larsson, M. W.; Mårtensson, T.; Sköld, N.; Svensson, C. P. T.; Wacaser, B. A.; Wallenberg, L. R.; Samuelson, L. *J. Cryst. Growth* **2004**, *272*, 211−220.
(39) Cooke, C.J.; Hume-Rothery, W. *J. Less-Common Met.* **1966**, *10*, 42.
(40) Poizot, P.; Laruelle, S.; Grugeon, S.; Dupont, L.; Tarascon, J .M. *Nature* **2000**, *407*, 496−499.
(41) Buffat, P.; Borel, J. P. *Phys. Rev. A* **1976**, *13*, 2287−2298.

(42) Ford, A. C.; Ho, J. C.; Chueh, Y. L.; Tseng, Y. C.; Fan, Z. Y.; Guo, J.; Bokor, J.; Javey, A. *Nano Lett.* **2009**, *9*, 360−365.
(43) Wiersma, R.; Stotz, J. A. H.; Pitts, O. J.; Wang, C. X.; Thewalt, M. L. W.; Watkins, S. P. *J. Electron. Mater.* **2001**, *30*, 1429−1432.
(44) Gutsche, C.; Regolin, I.; Blekker, K.; Lysov, A.; Prost, W.; Tegude, F. J. *J. Appl. Phys.* **2009**, *105*, 024305.
(45) Sørensen, B. S.; Aagesen, M.; Sørensen, C. B.; Lindelof, P. E.; Martinez, K. L.; Nygård, J. *Appl. Phys. Lett.* **2008**, *92*, 012119.
(46) Yang, Z. X.; Han, N.; Wang, F. Y.; Cheung, H.-Y.; Shi, X. L.; Yip, S. P.; Hung, T. F.; Lee, M. H.; Wong, C.-Y.; Ho, J. H. *Nanoscale* **2013**, *5*, 9671−9676.